Crystal growth and in-plane optical properties of $Tl_2Ba_2Ca_{n-1}Cu_nO_x$ $(n=1,2,3)$ superconductors

Y. C. Ma and N. L. Wang*
Beijing National Laboratory for Condensed Matter Physics, Institute of Physics, Chinese Academy of Sciences, Beijing 100080, People's Republic of China

(Received 11 March 2005; revised manuscript received 8 August 2005; published 28 September 2005)

Single crystals of thallium-based cuprates with the general formula $Tl_2Ba_2Ca_{n-1}Cu_nO_x$ $(n=1,2,3)$ have been grown by the flux method. The superconducting transition temperatures determined by the ac magnetic susceptibility are 92, 109, and 119 K for $n=1,2,3$, respectively. X-ray diffraction measurements and an EDX compositional analysis were described. We measured in-plane optical reflectance from room temperature down to 10 K, placing an emphasis on Tl-2223. The reflectance roughly has a linear-frequency dependence above the superconducting transition temperature, but displays a pronounced knee structure together with a diplike feature at higher frequency below T_c. Correspondingly, the ratio of the reflectances below and above T_c displays a maximum and a minimum near those feature frequencies. In particular, those features in Tl2223 appear at a higher-energy scale than Tl2212 and Tl2201. The optical data are analyzed in terms of the spectral function. We discussed the physical consequences of the data in terms of both clean and dirty limits.

DOI: 10.1103/PhysRevB.72.104518 PACS number(s): 74.25.Gz, 74.72.Jt

I. INTRODUCTION

Since the discovery of the high-temperature superconductors (HTSC) in the 1980s, many experiments have been done to disclose the microscopic origin of high-temperature superconductivity. For example, inelastic neutron scattering revealed a peculiar magnetic resonance mode at an energy of 41 meV in a two-dimensional reciprocal lattice position (π,π) for optimally doped $YBa_2Cu_3O_{6+x}$.[1,2] The angle-resolved photoemission spectroscopy (ARPES) has indicated a kink in the band dispersion as well as an anisotropic gap (the d wave behavior) for some high-T_c cuprates.[1,3,4] These results are very helpful for understanding the superconductivity mechanism in the cuprates. Naturally, one may ask whether these behaviors are generic in HTSC materials. But there are technical reasons why those experimental probes have not been used with success on all the families of HTSCs. For example, an inelastic neutron scattering experiment requires large-size single crystals and had mostly been done on YBCO-123 and LSCO-214,[1,2,5] although some groups have tried to work on $Tl_2Ba_2CuO_{6+\delta}$ by synthesizing about 300 relatively large (0.5 to 3 mm^3) single crystals and coaligning them in a mosaic of total volume 0.11 cm^3,[6] as well as on $Bi_2Sr_2CaCu_2O_{8+\delta}$ with a comparatively large single crystal of volume $10\times5\times1.2$ mm^3 and mosaicity (that is, the angular spread of the crystallographic axes), $\sim1°$.[7] Tunnelling spectroscopy and ARPES are surface-sensitive probes. They are mainly applied to Bi-based cuprate systems, as they could be cleaved easily in a vacuum along the Bi—O planes, yielding a high-quality virgin surface.[1] However, a technique like optical spectroscopy places relatively less demands on the sample size and surface, and have, consequently, been applied with success to a larger number of high-temperature superconducting systems. At present, optical probes cover a wide frequency and temperature range, which have provided much useful information about charge excitations and dynamics of cuprate superconductors.

In the whole HTSC families, thallium-based cuprates have provided a large series of superconductors including single Tl—O layered compounds with the number of CuO_2 layers from 1 to 5 and double Tl—O layered compounds $Tl_2Ba_2Ca_{n-1}Cu_nO_x$ with the CuO_2 layers n from 1 to 3 (hereafter abbreviated as Tl-2201, Tl-2212, Tl-2223, respectively).[8–15] The Tl-based cuprates offer a good opportunity to investigate the physical properties of systems with different number of CuO_2 layers in a unit cell, and therefore different T_c at the optimal doping. This will help us to understand the mechanism of high-temperature superconductivity. Another advantage of Tl-based cuprates is that all the double Tl—O layer based cuprates have higher T_c's than the double Bi—O layer-based cuprates with the same structure. Even for the single CuO_2-layered compound Tl-2201, its T_c can reach 90 K. Consequently, the difference between the superconducting state and the normal state can be easily probed. Nevertheless, despite those advantages, much less spectroscopic studies have been done on the Tl-based cuprates. This is mainly due to the difficulty of obtaining high-quality single crystal samples. One has to overcome the problem of avoiding the poisonous thallium volatility and the formation of intergrowth defects during crystal growth.[12] Infrared studies have been done on crystals of single-layered Tl-2201,[16,17] and thin films of double-layered Tl-2212,[18] but there is still no report, to the best of our knowledge, on triple-layered Tl-2223 and any other Tl-based superconductors.

We have recently successfully grown single crystals of $Tl_2Ba_2Ca_{n-1}Cu_nO_x$ compounds with $n=1$, 2, and 3 by the flux method. In this study, we first describe the crystal growth procedure and characterization of the as-grown crystals by the ac magnetic susceptibility, x-ray diffraction measurements, and EDX compositional analysis. Then, we report the measurement of the in-plane infrared reflectance. As optical data for optimally doped Tl-2201 and Tl-2212 are available in the literature, we place an emphasis on the spectra collected on triple-layered Tl-2223 crystals and their comparisons with the data of Tl-2212 and Tl-2201. Very similar

TABLE I. Nominal compositions in starting materials for crystal growth and transition temperatures of grown crystals Tl—Ba—Ca—Cu—O (Ref. 11).

Sample No.	Starting material Tl/Ba/Ca/Cu	T_c K	Size mm^2	Phase
A	2/2/0/1	92	1.2×1.5	Tl-2201
B	2/2/2/3	109	2.0×1.8	Tl-2212
C	2/2/6/6	119	1.2×0.9	Tl-2223

to Tl-2201 and Tl-2212, we observe a significant change of spectra after entering the superconducting state, which was related to the combination of a Boson mode and a gap. We analyzed the spectra in terms of the spectral function. A linear scaling is established between the energy of the characteristic feature and the superconducting transition temperature for different systems at optimal doping.

II. CRYSTAL GROWTH AND CHARACTERISTICS

Single crystals were grown by the flux method from raw materials with nominal compositions as listed in Table I. The mixed oxide BaCaCuO powders were synthesized prior to the crystal growth. For example, we made the BaCaCuO-223x powder for Tl-2212, and BaCaCuO-266x for Tl-2223. Then, Tl_2O_3 powder was added into the mixed powders to get a stoichiometry as in Table I. The ratio of the oxide powders is essential for the crystal phase growth.

In the growth experiment, the powders of amount ~15 g were ground in an agate mortar, then placed in an alumina crucible and covered with two Al_2O_3 lids for decreasing the volatility of Tl_2O_3. The crucible was put in a tube furnace with flowing oxygen, and heated up to a high temperature for several hours. The temperature was set to be different for growing Tl-2201, Tl-2212, and Tl-2223 systems, as shown in Fig. 1. The furnace was cooled down slowly at a rate of about 10 °C per hour to a certain temperature (depending on the system), then down to room temperature naturally. The oxygen flowed all the time during the sintering process. The starting temperature and the cooling rate seriously affect the

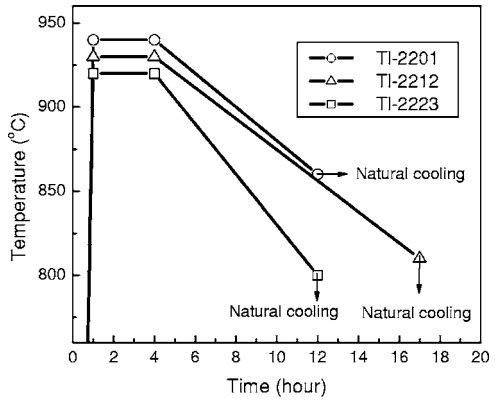

FIG. 1. The growth process for Tl-2201 (a), Tl-2212 (b), and Tl-2223 (c) single crystals.

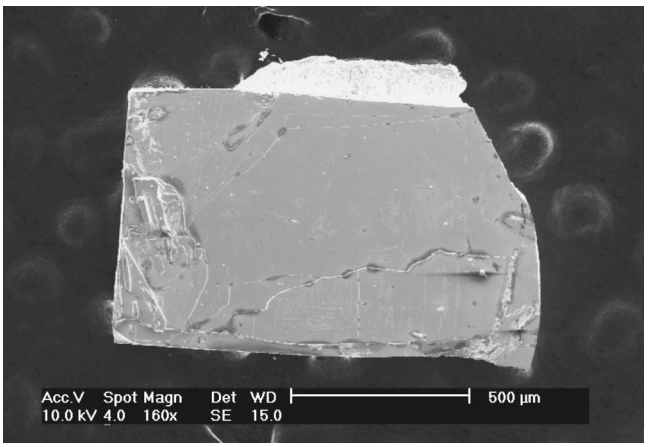

FIG. 2. SEM images of as-grown crystals Tl-2223.

size of an as-grown crystal. It also affects substantially the superconducting transition temperature of the Tl-2201 phase.

As the crucible had been cooled down to room temperature, the mm-sized crystals of Tl-2201, Tl-2212, and Tl-2223, single crystals have been formed. Some shiny, usually freestanding, crystals are found at the place near the cavities formed in the melt. The SEM image of a typical Tl-2223 crystal is shown in Fig. 2.

According to x-ray diffraction measurements shown in Fig. 3, nearly all the $(0,0,l)$ peaks can be seen clearly, furthermore, no other phase can be seen in the diffraction pattern, and every sample has a good c-axial orientation that is perpendicular to the sample natural growth face. The half-widths of the midpoint of the x-ray diffraction peaks are

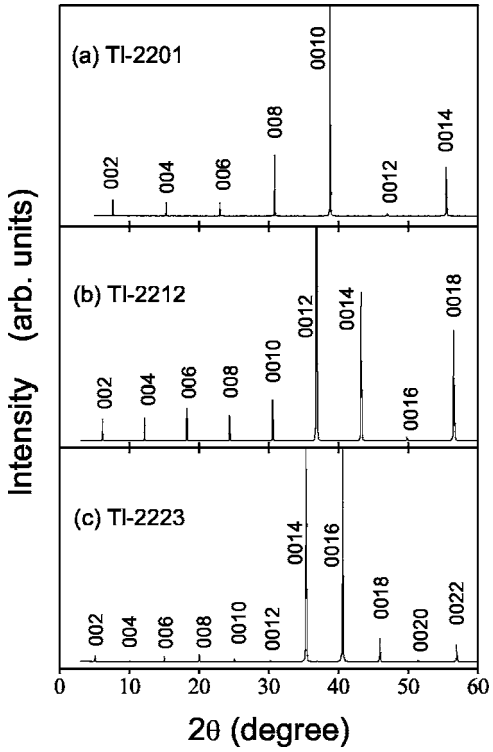

FIG. 3. The x-ray diffraction patterns up to 60 deg for (a) Tl-2201, (b) Tl-2212, and (c) Tl-2223.

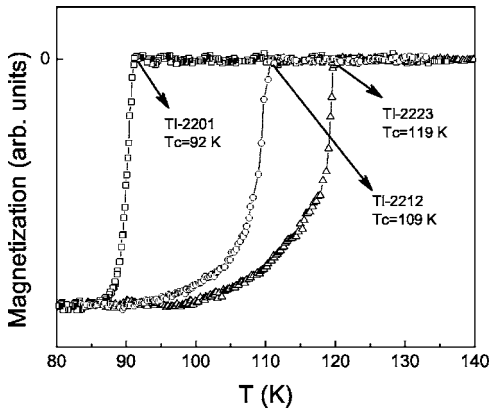

FIG. 4. Temperature dependence of ac susceptibility for Tl-2201, Tl-2212, and Tl-2223 single crystals. The maximum magnetization in each sample has been normalized.

typically 0.07°, 0.09°, and 0.08° for Tl-2201, Tl-2212, and Tl-2223 single crystals, respectively. Clearly the intergrowth defects of the different members have been depressed by the sintering process. The lattice constants, c, of the three type of crystals are 23.21, 29.28 and 35.55 Å for Tl-2201, Tl-2212, Tl-2223 phases, respectively, as there is a $CuCaO_2$ difference in each unit cell for the three phases.

The superconducting transition temperature T_c was determined by an ac susceptibility measurement. T_c increases in the three phases as the CuO_2 layers in a unit cell increase from 1 to 3. The T_c for as-grown Tl-2212 and Tl-2223 crystals are always close to 109 and 119 K, respectively, while the T_c for as-grown Tl-2201 crystals ranges from about 70 to 92 K. Figure 4 shows the temperature dependence of the ac susceptibility for as-grown Tl-2201, Tl2212, and Tl-2223 single crystals.

The compositions of the crystals were examined by energy dispersive x-ray microanalysis (EDX). The quantitative measurements were performed at several points on the surface of the crystal, which show a good uniformity of composition on the crystal surface. Typical EDX spectra obtained from each phase of the crystal are shown in Fig. 5. As expected form the ideal chemical formula of each phase, the peak ratios of CaKα/BaLα and CuKα/BaLα in the EDX spectra increased with the number of Cu—O layers in Tl compounds. Note that there is no Ca in the Tl-2201 phase; this is because we did not mix the CaO before this phase has been formed. Other peaks are of the Tl, Ba, Ca, Cu character spectrum. All these results are consistent with the x-ray diffraction experiments.

III. OPTICAL PROPERTIES

An optical spectroscopy measurement can yield rich information about the charge dynamics of a system. Intensive optical studies have been done on La-, Y-, and Bi-based cuprate systems; comparatively, much less optical investigations have been done on Tl-based systems. As we mentioned in the Introduction, infrared studies on the Tl-based systems have been performed only on single-layer and double-layer compounds near optimal doping. Therefore, in this work, we

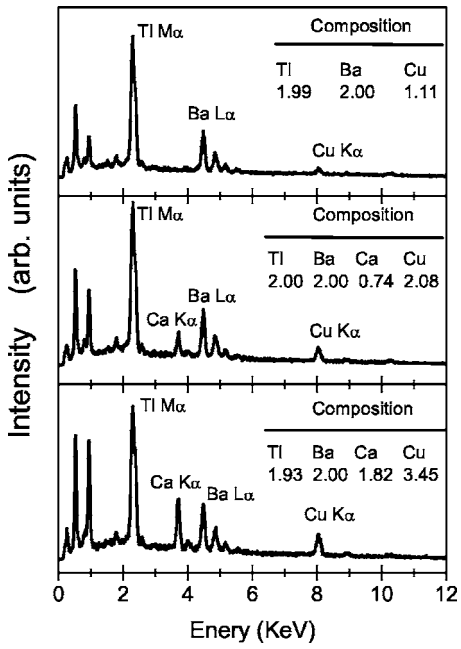

FIG. 5. EDX spectra and analyzed compositions for the Tl-2201 (a), Tl-2212 (b), and Tl-2223 (c) phases. The compositions are calculated on the assumption that the molar ratio of Ba is the ideal value of two.

shall mainly focus on the data of Tl-2223 crystals, as well as their comparisons with the data of Tl-2201 and Tl-2212.

The reflectance measurements from 100 to 22 000 cm^{-1} were carried out on a Bruker 66v/S spectrometer. An *in situ* overcoating technique was used for the experiment.[19] The optical conductivity spectra were derived from the Kramers-Kronig transformation. The Hagen-Rubens relation was assumed for the low-frequency extrapolation. At the high-frequency side, a constant extrapolation was adopted up to 100 000 cm^{-1}; then a $R(\omega) \sim \omega^{-4}$ was used. A comparison of the in-plane reflectances of Tl-2201, Tl-2212, and Tl-2223 single crystal at room temperature is shown in Fig. 6. Clearly, as the CuO_2 layers of a unit cell go from 1 to 3, the reflectance edge goes to higher energy. The observation indicates that the carrier density increases with an increasing in the number of CuO_2 layers in a unit cell.

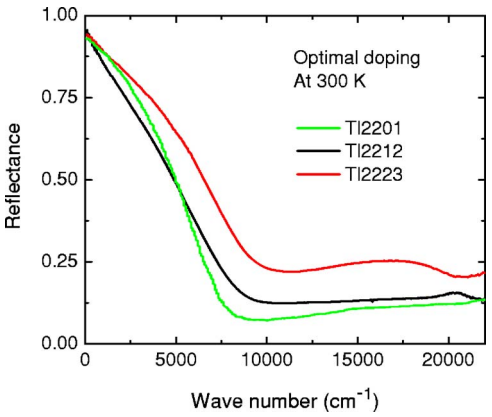

FIG. 6. (Color online) The reflectance data of Tl-2201, Tl-2212, and Tl-2223 crystals up to 22 000 cm^{-1} at room temperature.

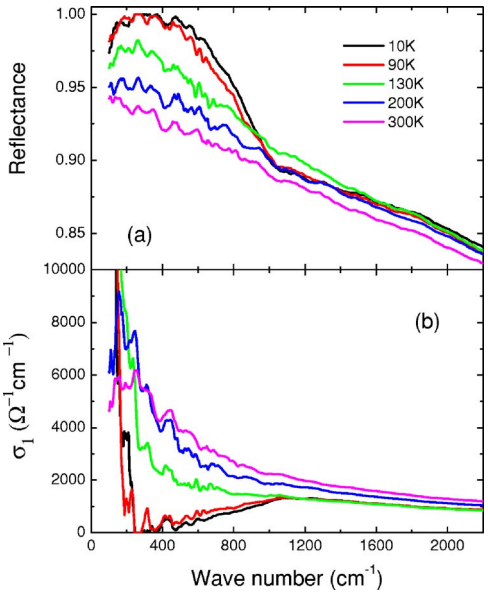

FIG. 7. (Color online) *ab*-plane optical data of the optimally doped Tl-2223 single crystal with $T_c = 119$ K. (a) The temperature-dependent reflectance and (b) the temperature-dependent $\sigma_1(\omega)$.

Figures 7(a) and 7(b) show the reflectance $R(\omega)$ and conductivity $\sigma_1(\omega)$ spectra for a Tl-2223 crystal at different temperatures. In the high temperature, the Tl-2223 reflectance spectra show roughly linear frequency dependence, a behavior common to all hole-doped high-T_c cuprates. The linear frequency dependence of $R(\omega)$ implies a linear variation of the inverse lifetime of carriers with frequency, which could be well described by a marginal Fermi liquid theory.[20] With decreasing temperature, the low-ω $R(\omega)$ increases, indicating a metallic response of the sample. At 10 K in the superconducting state, $R(\omega)$ shows a clear knee structure at around 600 cm^{-1}. Above this frequency, the reflectance drops fast and becomes lower than the normal-state values at around 1000 cm^{-1}. $R(\omega)$ recovers the linear-frequency dependence at a higher frequency of about 1600 cm^{-1}. Similar but slightly weak behaviors were seen at 90 K, which is close to T_c.

The temperature- and frequency-dependent optical responses of Tl-2201 and Tl-2212 crystals are very similar to those of Tl-2223 sample. For comparison we show in Fig. 8 the conductivity spectra for optimally doped Tl-2201, Tl-2212 and Tl-2223 at 300 K and 10 K, respectively. Qualitatively, the $\sigma_1(\omega)$ spectra exhibit the same characteristic in both normal and superconducting states for the three phases. The conductivity spectrum has a Drude-like shape in the normal state, but becomes suppressed below a certain frequency in the superconductiing state. However, it is found that the energy scale below which the $\sigma_1(\omega)$ is suppressed at 10 K shifts to lower frequencies as the CuO_2 layers in a unit cell decreases from 3 to 1.

In fact, the change of optical response in the superconducting state with respect to the normal state could be seen more clearly from the plot of the ratio of the reflectance below T_c over that above T_c. Figure 9 shows the ratio of $R_{10\ \mathrm{K}}(\omega)/R_{130\ \mathrm{K}}(\omega)$ as a function of frequency. The

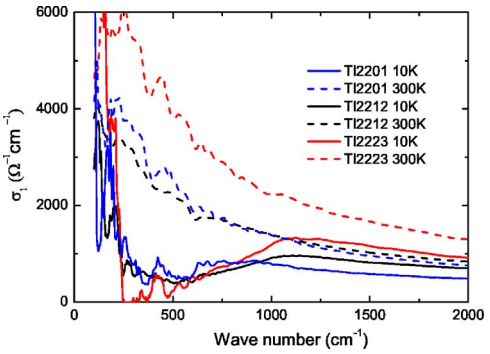

FIG. 8. (Color online) The low-frequency optical conductivity for the optimally doped Tl-2201, Tl-2212, and Tl-2223 samples at 300 and 10 K.

$R_{10\ \mathrm{K}}(\omega)/R_{95\ \mathrm{K}}(\omega)$ of a Tl-2201 crystal and the $R_{10\ \mathrm{K}}(\omega)/R_{120\ \mathrm{K}}(\omega)$ of a Tl-2212 crystal are also included for comparison. Obviously, both of them have a maximum and a minimum in the plot. The values near the maximum have much noise, nevertheless, we can see clearly the dip minimum and the fitting maximum of the Tl-2223 shift to higher energy compared with Tl-2212[18] and Tl-2201.

A useful way to display in-plane infrared data is in terms of the optical lifetime of the carriers that can be extracted from the conductivity data using the extended-Drude formalism. The reciprocal of the lifetime, or the scattering rate, $1/\tau(\omega)$, is defined as[17]

$$\tau^{-1}(\omega) = \frac{\omega_p^2}{4\pi}\frac{\sigma_1(\omega)}{\sigma_1^2(\omega)+\sigma_2^2(\omega)}, \tag{1}$$

where ω_p is the plasma frequency. The scattering rate $1/\tau(\omega)$ for 10, 130 K, and 300 K data are shown in Fig. 10, extracted from Eq. (1) using the plasma frequency 2.0×10^4 cm^{-1}, determined by summarizing the optical conductivity up to the plasma edge near 8000 cm^{-1}. The $1/\tau(\omega)$ at 300 K is linear in the low-energy range. However, $1/\tau(\omega)$ at 10 K exhibits a rapid rise and a substantial overshoot of the normal-state spectrum at the frequencies corresponding to the maximum and minimum in the $R_{10\ \mathrm{K}}(\omega)/R_{130\ \mathrm{K}}(\omega)$

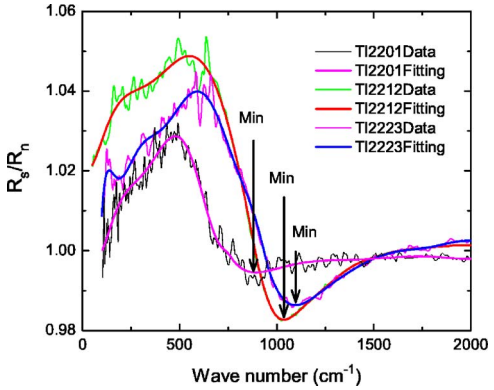

FIG. 9. (Color online) The $R_s(\omega)/R_n(\omega)$ from 100 to 2200 cm^{-1} of the optimally doped Tl-2223 single crystal with $T_c = 119$ K. The Tl-2201 and Tl-2212 data have been included in for comparison.

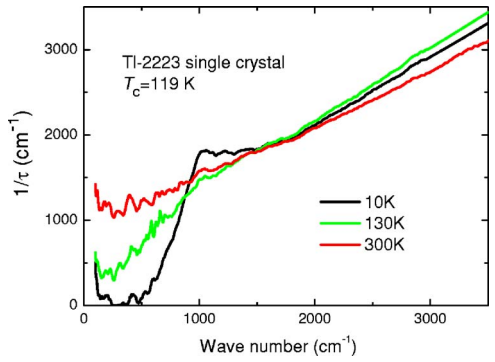

FIG. 10. (Color online) Optical scattering rate spectra from 100 to 3500 cm^{-1} of the optimally doped Tl-2223 single crystal with T_c=119 K.

plot (in Fig. 9), respectively. Above this range the scattering rate in the superconducting state becomes linear up to several thousand wave numbers.

The sharp rise and the overshoot in $1/\tau(\omega)$ at low T are quite similar to other high-T_c cuprates. The difference is that the energy scales of the characteristic features for Tl-2223 are higher than that for Tl-2212 compound. In our earlier study,[18] we already showed that the same structures in $1/\tau(\omega)$ on the Tl-2212 system with T_c=108 K are substantially higher than systems with T_c around 90 K. A comparison of the scattering rate for the three phases at 10 K is shown in Fig. 11. In this plot, the data for the Tl-2201 crystal near optimal doping are taken from Puchkov's work.[16] Our data on the Tl-2201 crystal are almost identical to their reported data. The energy shifts of both the sharp rise and the overshoot structures are seen rather clearly. In fact, the energy scales of those features continue to shift up in compounds with a higher superconducting transition temperature. This can be seen very clearly from the optical work done on Hg-1223 with $T_c \sim 130$ K.[21]

The characteristic features were widely believed to result from the interaction of electrons with a collective mode in combination with a superconducting gap that appears below

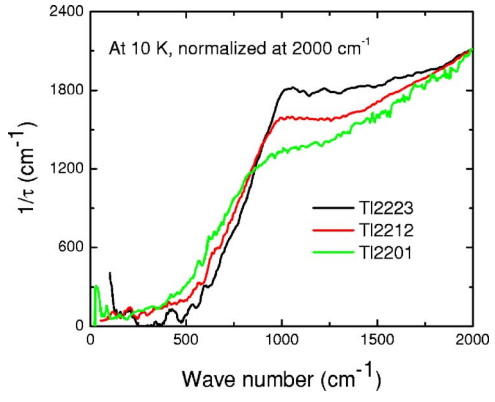

FIG. 11. (Color online) Optical scattering rate spectra from 200 to 2000 cm^{-1} of the optimally doped Tl-2201, Tl-2212, and Tl-2223 single crystals. Data for Tl-2201 with T_c=88 K (very close to the optimal doping) are taken from Ref. 16. The data have been normalized to Tl-2223 at 2000 cm^{-1}.

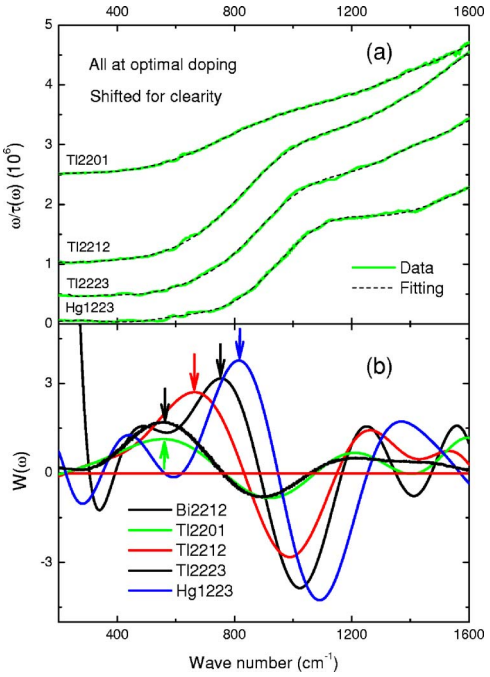

FIG. 12. (Color online) (a) Scattering rate data multiplied by ω for Tl-2201, Tl-2212, Tl-2223, and Hg-1223. The scattering data for Tl-2201 were taken from Ref. 16, the data for Hg-1223 from Ref. 21. The curves are shifted vertically for clarity. (b) The spectral function $W(\omega)$ at 10 K (in the superconducting state) derived from the polynomial fitting. The data for Bi-2212 were taken from Ref. 25. The arrows indicate the positions of main peaks.

T_c.[22–26] In a photoemission experiment, a kink in the dispersion along the zone diagonal develops in the low temperature that is due to the correction by the real part of self-energy of a quasiparticle, and by the Kramers-Kronig relation, a rapid broadening of the photoemission linewidth, i.e. a sudden change of the lifetime of a quasiparticle is seen simultaneously.[1] The enhanced absorption above the knee frequency in an infrared response results from an enhanced scattering, which should have the same origin as the linewidth broadening or the kink in the dispersion observed along the zone diagonal in ARPES. Extracting the bosonic spectral function from the infrared spectra has been established theoretically by performing the second derivative of the optical scattering rate multiplied by frequency through[22,27]

$$W(\omega) = \frac{1}{2\pi}\frac{d^2}{d\omega^2}\left(\omega\frac{1}{\tau(\omega)}\right). \quad (2)$$

As such, a second derivative contains detectable singularities at a number of characteristic energies, the inversion method was widely used to determine the parameters like gap amplitude Δ and Boson mode energy Ω.

Figure 12(a) shows the plot of the scattering rate multiplied by frequency versus frequency for Tl-2201, Tl-2212, and Tl-2223 crystals. The data for the Hg-1223 crystal taken from Ref. 21 are also plotted. In order to perform a second derivative, the curves were fit with a high-order (40 orders) polynomial. To see the energy scales of the features more

clearly, we have shifted the curves vertically for different compounds. The spectral functions $W(\omega)$ obtained by Eq. (2) are plotted in Fig. 12(b). The $W(\omega)$ data for a high-quality Bi-2212 crystal with T_c=91 K obtained by Tu *et al.* are also added.[25] We can see clearly that, roughly at frequencies corresponding to the sharp rise and the overshoot in $1/\tau(\omega)$, there exists a major peak, or positive maximum, as indicated by the arrow, and a negative minimum in $W(\omega)$, respectively. In particular, for those systems with different T_c at optimal doping, the positive maximum and the negative minimum increase systematically with T_c.

It also deserves to be remarked that some weak maxima could exist preceding the main peak in $W(\omega)$. They come from the weak fluctuations in the fitting curves due to the experimental noise in the far-infrared region. Because the signal-to-noise level at the low-ω side depends strongly on the sample size, those structures are observed most eminently for Tl-2223 and Hg-1223 samples due to their relatively smaller sizes. Those maxima are not steady for different measurements on different samples. Nevertheless, the main peak and the following negative minimum in each spectral function $W(\omega)$ are fairly robust. They correspond to the sharp rise and overshoot in the scattering rate spectra, or the knee structure and diplike feature in the reflectance spectra.

Although it is generally agreed that the second derivative of the optical conductivity, i.e. the $W(\omega)$ spectrum, reflects the bosonic spectral function, different opinions exist regarding to the energy positions of the positive maximum and the negative minimum. Considering a *d*-wave gap symmetry, Carbotte *et al.*[22,23] argued that the peak in $W(\omega)$ below T_c occurs at $\Delta+\Omega$, while the minimum is at $2\Delta+\Omega$. However, Abanov *et al.*[24] argued that the *d*-wave gap does not affect the threshold position in conductivity, as a result, a sharp maximum in $W(\omega)$ occurs at $2\Delta+\Omega$ followed by a deep minimum. They emphasized that at T=0 K the maximum and minimum are at the same frequency, while at a finite temperature, the maximum shifts to low frequency, but the minimum remains at the same frequency as at T=0 K. So, they also identify the $2\Delta+\Omega$ with the deep minimum in $W(\omega)$. If we accept that the peak in $W(\omega)$ is located at $\Delta+\Omega$, and the minimum is at $2\Delta+\Omega$, we obtained a plot for the peak and the dip energy as a function of T_c for the different systems at optimal doping, as shown in Fig. 13. Obviously, both of them scale well with T_c for different systems. Furthermore, the difference between them should give the superconducting gap energy Δ. In the figure, we also make the plot for the energy difference between the dip and the peak versus T_c for different compounds. It then shows a trend of the increase with a decrease of the superconducting transition temperature T_c for different systems. This result is not physically reasonable, and is also in contradiction to the ARPES[28,29] and Raman[30] experimental results, which show a decrease of the gap amplitude for the systems with lower T_c. We think that the current analysis puts a new challenge to the established models.

Nevertheless, the linear scaling of the energy of the peak (and also the dip) in $W(\omega)$ with T_c is firmly established in our experiment. At present, the nature of the mode is not clear. It

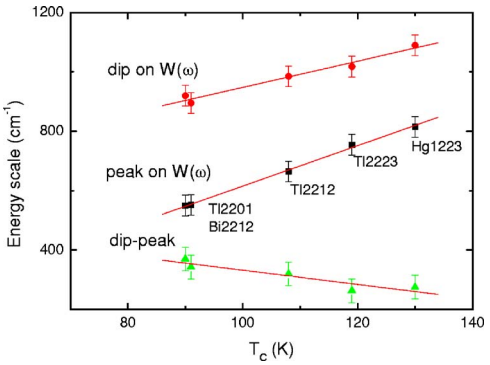

FIG. 13. (Color online) The energy scales of the negative dip and the main peak versus T_c for several optimally doped cuprates. The energy difference between the dip and the peak is extracted simply.

is still under dispute whether the mode is a phonon or a magnetic resonance, as detected by the neutron scattering experiment. If the maximum or minimum indeed involve a sum of the gap Δ and a Boson mode Ω, then the scaling behavior not only means that the gap amplitude Δ is proportional to T_c, but Boson mode energy Ω is also proportional to T_c for the different systems. In this case, the phonon origin for the Boson mode is unambiguously ruled out, because the in-plane phonon is determined by the Cu—O bond length, which should not change in systems with different T_c.

However, we would also like to point out that the above scenario of a mode plus a gap for the reflectance feature below T_c relies on the clean limit of the *ab*-plane superconductivity. The unreasonable result obtained from the energy difference between the dip and the peak in terms of the model by Carbotte *et al.*[22] may suggest that the *ab* plane of high-T_c cuprates may not be in the clean limit. In the case of a dirty limit, on the other hand, the sharp rise feature in the scattering rate should be at 2Δ, since the impuritie's elastic scattering should be able to transfer the momentum of the particle-hole excitations without affecting the threshold energy. At present, there is still no agreement on whether or not the *ab* plane is in a clean limit. Very recently, Homes[31] suggests that the criteria of a small value of the quasiparticle scattering rate for $T \ll T_c$ is not a good measure of whether or not the superconductivity is in the clean or dirty limit. By contrast, the normal-state value of $1/\tau$ should be considered when determining whether a system is in the clean or dirty limit. They also pointed out that the clean-limit requirement is much more stringent for a *d*-wave system than it is for a material with an isotropic energy gap, since it not only requires $1/\tau$, much less than the maximum gap amplitude, but also $1/\tau \leqslant 2\Delta_k$ in the nodal regions. They established a linear scaling relation $\rho_s \propto \sigma_{dc} T_c$ for cuprates,[32] and argued that this scaling is the hallmark of a dirty-limit system.[31] In a dirty-limit case, no boson mode would be involved in the sharp rise of the scattering rate, or the main peak in the spectral function $W(\omega)$. The feature would be purely due to the singularity of the density of state at the gap position. Then what we observed and analyzed in this work only reflects the variation of the gap amplitude in systems with different T_c. At present, it needs rather sufficient experimental data and

more theoretical efforts to identify whether the *ab*-plane superconductivity in cuprates is in the dirty limit.

IV. SUMMARY

Single crystals of thallium-based cuprates have been grown by the flux method. All crystals were of the platelet form, from 0.5 to 2 mm^2. They were characterized by ac susceptibility, x-ray diffraction, and a SEM and EDX analysis. The optical properties were investigated for the crystals with focus on the Tl-2223 compounds. The reflectance spectrum exhibits a knee structure at around 600 cm^{-1} and a dip at a higher frequency below T_c. The ratio of the reflectance below and above T_c displays a maximum and pronounced minimum at the knee and dip frequencies. The scattering rate and its second derivative were extracted and compared with other cuprate systems. A linear scaling behavior for the maximum and the negative minimum with T_c is established for systems with different T_c at optimal doping. We discussed the physical consequences of the experimental data in terms of both clean and dirty limits. At present, it is an open question whether the *ab* plane of HTSCs is in the clean or dirty limit.

ACKNOWLEDGMENTS

We wish to acknowledge H. Chen for her help in the XRD experiment. This work is supported by the Ministry of Science and Technology of China (973 project No: 2006CB601002), the National Science Foundation of China, the Knowledge Innovation Project of Chinese Academy of Sciences.

*Electronic address: nlwang@aphy.iphy.ac.cn

[1] M. R. Norman and C. C. Pépin, Rep. Prog. Phys. **66**, 1547 (2003).
[2] H. A. Mook, M. Yethiraj, G. Aeppli, T. E. Mason, and T. Armstrong, Phys. Rev. Lett. **70**, 3490 (1993).
[3] H. Ding, T. Yokoya, J. C. Campuzano, T. Takahashi, M. Randeria, M. R. Norman, T. Mochiku, K. Kadowaki, and J. Giapintzakis, Nature **382**, 51 (1996).
[4] A. G. Loeser, Z. X. Shen, D. S. Dessau, D. S. Marshall, C. H. Park, P. Fournier, and A. Kapitulnik, Science **273**, 325 (1996).
[5] S. W. Cheong, G. Aeppli, T. E. Mason, H. Mook, S. M. Hayden, P. C. Canfield, Z. Fisk, K. N. Clausen, and J. L. Martinez, Phys. Rev. Lett. **67**, 1791 (1991).
[6] H. He, P. Bourges, Y. Sidis, C. Ulrich, L. P. Regnault, S. Pailhes, N. S. Berzigiarova, N. N. Kolesnikov, and B. Keimer, Science **295**, 1045 (2002).
[7] H. F. Fong, P. Bourges, Y. Sidis, L. P. Regnault, A. Ivanov, G. D. Gu, N. Koshizuka, and B. Keimer, Nature **398**, 588 (1999).
[8] S. S. P. Parkin, V. Y. Lee, A. I. Nazzal, R. Savoy, T. C. Huang, G. Gorman, and R. Beyers, Phys. Rev. B **38**, 6531 (1988).
[9] H. Ihara, R. Sugise, K. Hatashi, M. Terada, M. Jo, N. Hirabayashi, A. Negishi, N. Atoda, H. Oyanagi, T. Shimomura, and S. Ohashi, Phys. Rev. B **38**, 11952 (1988).
[10] Z. Z. Sheng and A. M. Hermann, Nature **332**, 138 (1988).
[11] T. Kotani, T. Kaneko, H. Takei, and K. Tada, Jpn. J. Appl. Phys. **28**, 1378 (1989).
[12] A. Maignan, C. Martin, V. Hardy, Ch. Simon, M. Hervieu, and B. Raveau, Physica C **219**, 407 (1994).
[13] S. Kondoh, Y. Ando, M. Onoda, and M. Sato, Solid State Commun. **65**, 1329 (1988).
[14] S. S. P. Parkin, V. Y. Lee, E. M. Engler, A. I. Nazzal, T. C. Huang, G. Gorman, R. Savoy, and R. Beyers, Phys. Rev. Lett. **60**, 2539 (1988).
[15] N. Merrien, L. Coudrier, C. Martin, A. Maignan, F. Studer, and A. M. Flank, Phys. Rev. B **49**, 9906 (1994).
[16] A. V. Puchkov, T. Timusk, S. Doyle, and A. M. Hermann, Phys. Rev. B **51**, 3312 (1995).
[17] A. V. Puchkov, D. N. Basov, and T. Timusk, J. Phys.: Condens. Matter **8**, 10049 (1996).
[18] N. L. Wang, P. Zheng, J. L. Luo, Z. J. Chen, S. L. Yan, L. Fang, and Y. C. Ma, Phys. Rev. B **68**, 054516 (2003).
[19] C. C. Homes, M. Reedyk, D. A. Crandles, and T. Timusk, Appl. Opt. **32**, 2976 (1993).
[20] J. Hwang, T. Timusk, A. V. Puchkov, N. L. Wang, G. D. Gu, C. C. Homes, J. J. Tu, and H. Eisaki, Phys. Rev. B **69**, 094520 (2004).
[21] J. J. McGuire, M. Windt, T. Startseva, T. Timusk, D. Colson, and V. Viallet-Guillen, Phys. Rev. B **62**, 8711 (2000).
[22] J. P. Carbotte, E. Schachinger, and D. N. Bosov, Nature **401**, 354 (1999).
[23] E. Schachinger and J. P. Carbotte, Phys. Rev. B **64**, 094501 (2001).
[24] A. Abanov, A. V. Chubukov, and J. Schmalian, Phys. Rev. B **63**, 180510(R) (2001).
[25] J. J. Tu, C. C. Homes, G. D. Gu, D. N. Basov, and M. Strongin, Phys. Rev. B **66**, 144514 (2002).
[26] J. Hwang, T. Timusk, and G. D. Gu, Nature **427**, 714 (2004).
[27] F. Marsiglio, T. Startseva, and J. P. Carbotte, Phys. Lett. A **245**, 172 (1998).
[28] H. Matsui, T. Sato, T. Takahashi, H. Ding, H.-B. Yang, S.-C. Wang, T. Fujii, T. Watanabe, A. Matsuda, T. Terashima, and K. Kadowaki, Phys. Rev. B **67**, 060501(R) (2003).
[29] D. L. Feng, A. Damascelli, K. M. Shen, N. Motoyama, D. H. Lu, H. Eisaki, K. Shimizu, J.-i. Shimoyama, K. Kishio, N. Kaneko, M. Greven, G. D. Gu, X. J. Zhou, C. Kim, F. Ronning, N. P. Armitage and Z.-X. Shen, Phys. Rev. Lett. **88**, 107001 (2002).
[30] Y. Gallais, A. Sacuto, and D. Colson, Physica C **408**, 785 (2004).
[31] C. C. Homes, S. V. Dordevic, T. Valla, and M. Strongin arXiv, cond-mat/0410719.
[32] C. C. Homes, S. V. Dordevic, M. Strongin, D. A. Bonn, R. X. Liang, W. N. Hardy, S. Komiya, Y. Ando, G. Yu, N. Kaneko, X. Zhao, M. Greven, D. N. Basov, and T. Timusk, Nature **430**, 539 (2004).